*International Journal of Engineering Applied Sciences and Technology, 2022*
**Vol. 7, Issue 4, ISSN No. 2455-2143, Pages 262-275**
Published Online August 2022 in IJEAST (http://www.ijeast.com)

# ADVANCE CATALYST MATERIALS FOR HYDROGEN FUEL CELLS

Pranav Sawant, Amartya Singh, Kartik Wagh, Pranjal Shrivastava
Department of Chemical Engineering,
Vishwakarma Institute of Technology, Pune, India

***Abstract*— Catalytic Engineering plays a dominant role in increasing the catalytic activity of the catalysts in the Hydrogen Fuel Cells. This paper gives detailed description about different catalytic engineering techniques to increase the intrinsic activity of the active sites. These techniques have given promising results for reducing the cost and improving the performance of the catalysts. In the later section of this paper review on the growth of Platinum Nanowires in One Dimension is provided developed in order to increase the catalytic activity of PEMFC. The modeling and simulations of a typical PEMFC cell is done to illustrate the working of the fuel cells and different factors that affect the efficiency of PEMFC.**

***Keywords*— PEMFC, Catalyst, Nano architecture, Pt Nano wire and Mathematical Modulation and Simulation.**

## I. INTRODUCTION

Hydrogen is an important chemical material that is utilized in a large scale in synthetic chemical industries in modern society. The Hydrogen Fuel cells offer a significant advantage over traditional combusting based thermal energy conversion, so they provide efficiencies of electrical power supply in the range of 35 to 55%, causing very low level of pollutant emission. They can be used in a wide variety of applications from miniaturized portable power to stationary power stations.
There will be a high demand of Hydrogen Fuel Cells in the coming decades. As there will be various problems faced by the manufacturers of the fuel cell for the transportation, efficiency and storage of hydrogen in the fuel cells. The project undertaken is to study various methods through which the efficiency of the hydrogen fuel cells could be increased as a whole. The major part of the study focus on the catalysts used in the fuel cells.
The study is based on the reviewing various research papers, books and blogs about the current research in the field of catalysis for hydrogen fuel cells. This will give us the present updates and give opportunity to club few methods that can improve the efficiency of the hydrogen fuel cell.
Humans have started to broaden the thinking about the current climate crisis and have started movement to switch towards non-renewable sources of energy. The use of solar cells and electricity in the automobile industry have been a talk for about a decade and now we can see many companies switch to electric automobiles instead of regular one's. But now, it has come to picture that the efficiency and cost of the cells is a major problem faced by the manufacturers. It's quite reasonable to search for more options regarding the fuel cells and that's were hydrogen fuel cell powered vehicles come in to picture. Since Hydrogen Fuel cells are newest into the automobile industry a lot of research has to be done regarding the efficiency and its capacity.
The objective of this project is to study various factors affecting the catalytic activity inside the hydrogen fuel cell. T o achieve this research is done on the following topics (1) Improving intrinsic activity of the catalysts (2) Effect of alloying mechanism on catalytic activity (3) Use of Pt nanowire as a catalyst
The modeling and simulation gives an actual idea about the efficiency of a particular technique. Thus, at later sections we have provided the modeling and simulation of hydrogen fuel cell (PEMFC). The detailed description along with plots is also provided.
.

## II. CATALYST

One of the vital components of a PEMFC is the electrodes; the catalysts in PEMFC are present in electrodes. The catalyst used is platinum which is very costly as compared to other parts of PEMFC.
Every reaction needs some base energy for the reaction to begin; similarly in this case also some activation energy is required for the reaction to start. To do this in PEM fuel cell Platinum is used as a catalyst.
The surface area of a catalyst and the rate of reaction both are directly proportional to each other, because the reactions in PEMFC occur at surface of catalyst. Hydrogen is separated into electrons giving Hydrogen ion on the anode and oxygen is present at the cathode. The hydrogen ion combines with oxygen to produce water at the cathode. In order for these two reactions to occur it is necessary for the reactants to overcome energy barriers, for this the catalysts are used.

### 2.1 Designing an electrocatalyst for hydrogen-water conversion

Through Chemical Kinetics we know that the activation energy for the reaction is Gibbs free energy (DGact) and it is defined by the change in energy (Dmax). This change in Gibbs free energy is calculated in the rate determining step of the reaction which is at equilibrium. We have drawn a graph between the electrode material and activation energy(Fig-1).

*International Journal of Engineering Applied Sciences and Technology, 2022*
**Vol. 7, Issue 4, ISSN No. 2455-2143, Pages 262-275**
Published Online August 2022 in IJEAST (http://www.ijeast.com)

In PEMFC, the first step of the reaction is the reactant to get adsorbed on the surface of the catalyst. The second step involves, formation of hydrogen molecules by coupling with a proton and electron in the electrolyte.
The overall rate of the adsorption is decided by the rate determining step. If the rate of adsorption is high then it will cause a problem in overall reaction since breaking the metal-hydrogen bonds will be extremely difficult.

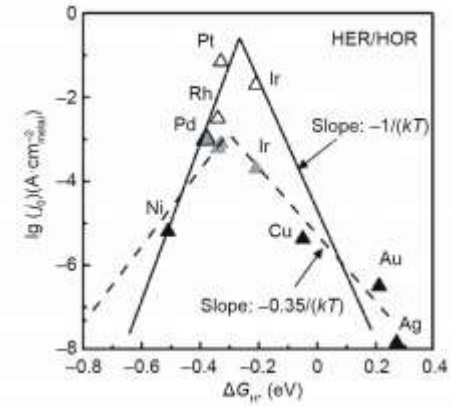


Figure 1.Volcano plot computing the DGH as a function of the surface normalized Hydrogen Evolution Reaction/Hydrogen Oxidation Reaction exchange current densities measured in acidic medium.

There are few metal who bind oxygen very firmly, in that case the rate is normalized by removing the oxygen ions and hydroxide ions. On contrary there are few metals that bind oxygen very delicately; in this case the rate of reaction is normalized by breaking of oxygen-oxygen bonds.
Therefore to achieve the optimum rate of reaction the catalyst should not bind the reaction very firmly or very delicately. Another ideology can be used apart from decreasing the activation energy barrier, i.e. by increasing the current density per unit area. Increase in current density ensures that more number of catalytic sites will be available for the reaction. The catalyst having rough surface has more number catalytic site for the reaction therefore increasing the current density per unit area over a rough surfaced catalyst will ensure that more number catalytic site will be available for the reaction to occur as compared to even surfaced catalysts. It can be inferred that, the activity of the electrode does not increase linearly with the amount of catalyst. It is dependent on other factors as well such as:
① Intrinsic activity of each active site present in the catalyst
② Density of active sites of a catalyst on a given electrode.

Improving the intrinsic activity of each active site is the most efficient way to ensure high activity of the catalyst. This can be done by studying the material's atomic structure and properties.

**2.2 Materials design for electrochemical hydrogen–water conversion**

**2.2.1 Nano architecture**

Nano architecture is a technique used to change the structure of materials at nanoscale. Nanoarchitecture have produced promising results since last decade and is currently a topic researched with great interests. Using nanoarchitecture we can change the properties of materials intrinsically or extrinsically. Using the similar technique optimization of electrocatalysts can be achieved. In the late 19$^{th}$ century, Prof. Brown. found that an alloy surface is generally rougher than that of a single metal, and can provide more active sites for a catalytic reaction. With booming research and development of synthesis techniques, many electrocatalytic nanomaterials have been manufactured including nanocages, nano-needles nanofibers, nanonets nanoflowers, nano-foam, nano-rings, nano-shells, and nanowires

**2.2.2 Facet engineering**

Facet engineering is another method to increase the catalytic activity. Certain materials have higher reactivity at particular facets because of rough surfaces and more number active sites available. The exposed facet(s) of a nanomaterial directly relate to the shape of the nanoparticle.
The surface morphology of Platinum(hkl) with well-defined surfaces was confirmed by scanning tunnelling microscopy (Scanning Transmission Microscopy, Figure 2).

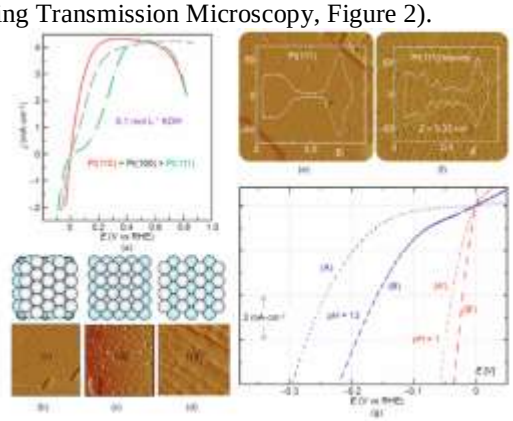

Figure 2 (a) Hydrogen Evolution Reaction /Hydrogen Oxidation Reaction on different facet surfaces of Platinum; (b–d) Scanning Transmission Microscopy images of different facets of Pt (the insets are their corresponding structural models Scanning Transmission Microscopy images for (e) the prepared Platinum(111) and (f) the Platinum islands/Platinum(111) surface; (g) the Hydrogen Evolution Reaction electrochemical responses of the two Platinum facets. (a–d) reproduced from Ref. [46], (e, f) reproduced from Ref. [47].

Low-coordinated atoms have a high density due to the steep edges present in the compound. Such metals with low coordination with high-index facets have very high catalytic

*International Journal of Engineering Applied Sciences and Technology, 2022*
**Vol. 7, Issue 4, ISSN No. 2455-2143, Pages 262-275**
Published Online August 2022 in IJEAST (http://www.ijeast.com)

reactivity as compared to that with the low index materials. Accordingly, the synthesis of high-index faceted nanomaterials has become a major task. In the last few years, enormous amount of research is done for the producing metallic nanomaterials with facets having high index to increase the catalytic reactivity. To reduce the cost of the catalyst designing of catalysts materials at nanoscale is done such as to expose particular facet(s) of the material.

**2.2.3 Amorphization**

Amorphization to modulate the atomic scale arrangement, and thus increase the catalytic performance, is another research hotspot. Short-range atomic arrangements of active sites.

In addition to the Hydrogen Evolution Reaction catalysis, Smith et al. demonstrated that amorphous materials are more active than the comparable crystalline materials for Oxygen Evolution Reaction catalysis, based on a study of the mixed-metal oxides of iron, nickel (Ni), and cobalt (Co). Due to the amorphous structure, the distribution of the metals in the amorphous films is homogeneous and their compositions can be accurately controlled.

Although the active sites of amorphous catalysts can be greatly enhanced by amorphous engineering, the electrical conductivity of the amorphous materials will be decreased due to short-range disorder in the crystal structure. Coupling these low-conductive materials with highly conductive materials is an effective route to guarantee the excellent electrocatalytic performance of amorphous catalysts.

**2.2.4 Alloying**

Alloying is the process of combining two or more metals or nonmetals with metals. Metal alloying is an effective method for improving the performance of metal catalysts. Through alloying we can increase the number of active as well as decrease the amount of a particular metal. (e.g., Platinum, Gold, Silver) which will result in decreasing the overall cost of the catalyst. Due to involvement of different metals, their catalytic properties can be inhered in the catalytic alloy.

According to the Brewer–Engel valence bond theory, alloying a metal with an unfilled d orbital and a metal with internally paired d-electrons can modulate the hydrogen adsorption energy on the alloy surface, thus improving the hydrogen evolution activity.

To reduce the cost of the catalyst several metals like Cobalt, Nickle, Iron, Copper, Vanadium etc are combined with noble metals to form alloys as electrocatalysts. Studies of ORR performances on Platinum-Metal alloys revealed the following activity order: PtFe/C >PtCo/C >PtV/C >PtNi/C > Pt/C. The following stability order was also determined: Pt3Ir > Pt3Co > Pt3Ni > Pt3Fe. According to that study, the ORR mechanism on Pt3M catalysts was either O2 dissociation or proton/electron transfer to molecular O2, and the optimal ORR catalyst should have a weaker oxygen-binding energy than Pt. Bampos et al. further synthesized a series of carbon supported Pd–M (where M = Ag, Co, Cu, Fe, Ni, or Zn) bimetallic catalysts as ORR electrocatalysts in acidic solution. The ORR activity of these Pd-based alloys was found to descend as follows: PdZn/ C >PdNi/C > Pt/C >PdAg/C PdCo/C >PdFe/C >PdCu/C > Pd/C. Notably, PdZn/C exhibited a specific activity three times higher than Pt/C at a potential between 0.35 and 0.5 V versus Ag/AgCl.

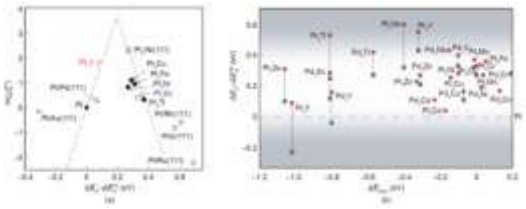

Figure 3 (a) This plot shows the relationship of kinetic current density VS the energy required to adhere oxygen (b) DEO of Pt on the surface of Pt-based alloys vs alloying energy.

**2.2.5 Growth of ultrathin Pt nanowires on single-layered Ni(OH)2.**

In this section, we review a strategy to design which is involved in the growth of one dimensional, ultrathin Pt nanowires on two dimensional $Ni(OH)_2$ nanosheets to increase the catalytic activity in basic solution. We illustrate that single-layered $Ni(OH)_2$ (SL-$Ni(OH)_2$) nanosheets with the required modifications on the surface are the key factors for development of Pt NWs (defined as Pt NWs/SL-$Ni(OH)_2$), and the obtained Pt NWs/SL-$Ni(OH)_2$ Stability and reactivity of hybrid catalyst are unknown in basic medium since the acid medium is most commonly used. In comparison with existing zero dimensional Pt nanoparticles (NPs), One Dimensional ultrathin Pt nanowires have very high active sites and smooth crystalline planes which provides the opportunity to improve the catalytic activity. Also, a large contact area between Pt NWs and the Ni(OH)2 substrates can effectively increase the possible agglomeration and transfer of Pt NWs and thus benefiting opportunity of the catalytic stability.

The synthesis procedure of Platinum Nano Wires/SL-$Ni(OH)_2$ is schematically presented in Fig. 4 First, finely dispersed SL-$Ni(OH)_2$ nanosheets in formamide were prepared by exfoliation of layered Ni(OH)2 intercalated with dodecyl sulfate(DS) ions. The single-layered nature of the exfoliated SL-Ni(OH)2 nanosheets was confirmed by the corresponding atomic force microscopy (AFM) measurement. Subsequently, 300 ml K2PtCl4 (60 mM) and 50 ml POTASSIUM HYDROXIDE (5 M) aqueous solutions were added to 10 ml SL-Ni(OH)2 formamide dispersion (0.5 mg ml 1), respectively. At last, the mixture was subjected to solvothermal treatment in a 20-ml Teflon-lined autoclave at 120 C for 4 h to obtain the Platinum Nano Wires/SL-Ni(OH)2 hybrids. Figure 4 represents the classic transmission electron microscopy images of Platinum Nano Wires/SL-Ni(OH)2 as synthesized products. It is also inferred that about 94% Platinum nanostructures are One Dimensional ultrathin

*International Journal of Engineering Applied Sciences and Technology, 2022*
**Vol. 7, Issue 4, ISSN No. 2455-2143, Pages 262-275**
Published Online August 2022 in IJEAST (http://www.ijeast.com)

nanowires with the uniform diameters of B1.8 nm and varying lengths of 10 to 50 nm.

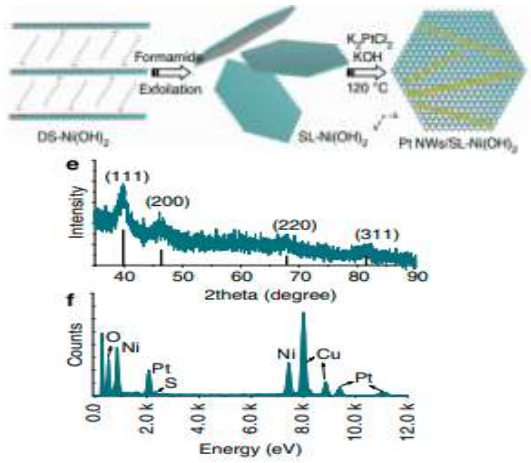


Figure 4 (Method for synthesis of Pt NWs/SL-Ni(OH)2; (e)XRD pattern of Pt NWs/SL-Ni(OH)2 (f) EDX spectrum of Pt NWs/SL-Ni(OH)2.

The characteristic determining the crystalline structure of Platinum NWs are looked into with the help of X-ray diffraction (XRD) pattern, in which the diffraction peaks can be indexed to, reflections of face centred cubic (fcc) Pt, respectively (Figure 4 ).

The XRD result also excludes formation of Platinum-Nickel alloy. The Ni(OH)2-Pt contact area in Pt NWs/SL-Ni(OH)2 is qualitatively measured by determining the electrochemical surface area (ECSA) of Pt NanoWires within Platinum NanoWires/SL-Ni(OH)2 and Platinum NanoWires completely exposed after removing SL-Ni(OH)2. The contacted part of Platinum NanoWires with SL-Ni(OH)2 deduced from their ECSA result is B35%, and hence the exposed Platinum atoms account for B65%. In addition to the shape and structure, the composition and chemical state of Platinum NWs/SL-Ni(OH)2 are recognized by energy dispersive X-ray (EDX) spectrum (Fig. 4) and X-ray photoelectron spectroscopy (XPS) (Fig. 5). The EDX analysis clearly distinguishes Platinum element from Platinum NanoWires, as well as O and Ni elements from SL-Ni(OH)2 nanosheets.

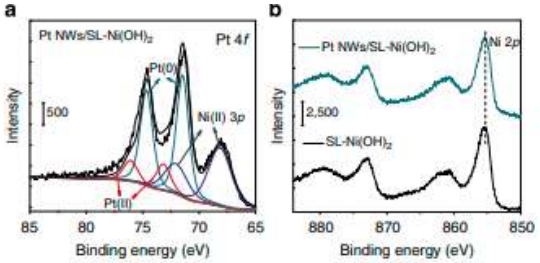


Figure 5| XPS analysis of Pt NWs/SL-Ni(OH)2. (a) XPS spectrum of Pt 4f region of Pt NWs/SL-Ni(OH)2; (b) XPS spectra of Ni 2p region of Pt NWs/ SL-Ni(OH)2 and SL-Ni(OH)2. The dashed line in (b) highlights that the Ni 2p peak position in the two samples remains the same

It is found that the reduction rate of Platinum precursors by formamide is decreased as the amount of POTASSIUM HYDROXIDE is increased. In the absence of POTASSIUM HYDROXIDE, large amount of Platinum NanoPores is rapidly formed outside the SL-Ni(OH)2 nanosheets; 5 M POTASSIUM HYDROXIDE solution into 10 ml of 0.5 mg ml 1 SL-Ni(OH)2 formamide dispersion gives rise to production of spherical Platinum NanoPores with average diameter of B3.2 nm on surface of SL-Ni(OH)2., whereas the reduction of Platinum precursors by formamide is hardly happened even after 12 h in the presence of excessive amount of POTASSIUM HYDROXIDE (that is, 100 ml of 5 M POTASSIUM HYDROXIDE solution was added in 10 ml of 0.5 mg ml 1 SL-Ni(OH)2 formamide dispersion), the reaction temperature and duration also have large impact on the final products. The aggregates of ultrathin Platinum Nanowires are formed when the reaction time is increased from 4h to 12h at 120$^{o}$C, while Platinum Nanopores assemblies are produced when the reaction temperature is increased from 120$^{o}$C to 140$^{o}$C under 4h reaction. This result indicates that the progressive decomposition of SL-Ni(OH)2 nanosheets in the formamide occurs during solvothermal reaction, most likely owing to coordination of N groups of formamide molecules with Ni2 þ ions of SL-Ni(OH)2 nanosheets.

Both DS-intercalated Ni(OH)2 nanosheets without fully exfoliation and carbonate (CO3 2 )-intercalated Ni(OH)2 multilayered nanosheets are prepared as the contrast substrates to compare with SL-Ni(OH)2 nanosheets. It is evident that as for DS-intercalated Ni(OH)2 nanosheets without fully exfoliation, Pt NP aggregates are produced and separated from the Ni(OH)2 nanosheets. 5 nm are grown on the surfaces of CO3 2 - intercalated Ni(OH)2 multilayered nanosheet. On the basis of the above results from the control experiments, we state that SL-Ni(OH)2 nanosheets directly affect the formation of Platinum Nanowires.

**2.2.6 Electrocatalytic performance of Pt NWs/SL-Ni(OH)2.**

The Hydrogen Evolution Reaction of electro-catalytic activity of as-synthesized Pt NWs/SL-Ni(OH)$_2$ is evaluated (Fig. 6a,b). In comparison, the electrocatalytic activities of other typical nanocatalysts including commercial Platinum catalyst (Johnson Matthey, 20 wt.% Pt on activated carbon, referred to Pt/C), Pt NPs/SL-Ni(OH)2 and pure ultrathin Pt Nanowires were also studied in the same parameters. Pure ultrathin Platinum NanoWires with average diameter of B2.0 nm. The Hydrogen electrode reaction activity of Platinum NanoWires/SL-Ni(OH)2 is approximately higher than a magnitude of 1 than that of the commercially available Platinum/Carbon catalyst. Also for the Platinum/Carbon catalyst modified by electrochemically deposited Ni(OH)2 (Pt/C@Ni(OH)2), the Hydrogen Evolution Reaction is still quite deep below that of Platinum Nanowiress/SLNi(OH)2.

*International Journal of Engineering Applied Sciences and Technology, 2022*
**Vol. 7, Issue 4, ISSN No. 2455-2143, Pages 262-275**
Published Online August 2022 in IJEAST (http://www.ijeast.com)

Apart from that, the Hydrogen Evolution Reaction electrocatalytic activity in less alkaline condition (0.1 M POTASSIUM HYDROXIDE) is tested (Fig. 6 b), and surprisingly the Hydrogen Evolution Reaction current density at Platinum NanoWires/SL-Ni(OH)2 (6.31 mA cm 2 at 0.07 V versus RHE) is also very high than that at Platinum NanoPores/SL-Ni(OH)2 (1.86 mA cm 2), commercial Platinum/Carbon (0.662 mA cm 2) and pure Platinum NanoWires (0.969 mA cm 2) The mass current density (at 0.07 V versus RHE) of Platinum NanoWires/SL-Ni(OH)2 is 0.679 mAmgPt 1 in 1 M POTASSIUM HYDROXIDE and 1.59 mAmgPt 1 in 0.1 M POTASSIUM HYDROXIDE solution, which is 4.35 and 4.50 times than that of commercial Platinum/Carbon, respectively.

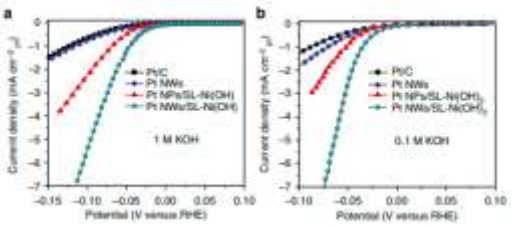


Figure6(a) Hydrogen Evolution Reaction activity of Platinum NanoWires/SL-Ni(OH)2, Platinum NanoPores/SL-Ni(OH)2, (b) Platinum NanoWires and commercial Platinum/Carbon (20 wt.%) in 0.1 M POTASSIUM HYDROXIDE at room temperature.

The reason for the superior Hydrogen Evolution Reaction activity of Pt NWs/SL-Ni(OH)2 in basic condition should be ascribed to two major factors:
(i) Combination of Platinum with Ni(OH)2 greatly enhances the Hydrogen Evolution Reaction activity of Platinum species (Platinum NanoWires/SL-Ni(OH)2 versus commercial Platinum/Carbon and pure Platinum NanoWires). In the hybrid systems, Ni(OH)2 substrates can effectively activate the hydroxide and hydrogen bonds, which restrict the limited capability of Platinum in H2O dissociation in basic solution for Hydrogen Evolution Reaction.
(ii) Ultrathin One Dimensional Platinum NanoWires can be exposed greater number of active sites paralleling maintaining improved electrons transport characteristics. Smaller charge transfer resistance of Platinum NanoWires/SL-Ni(OH)2 confirmed by electrochemical impedance spectroscopy further demonstrates this improved electron transport property in One Dimensional Platinum NanoWires. Lastly, the stability of Platinum NanoWires/SL-Ni(OH)2, Platinum NanoPores/Ni(OH)2, pure Platinum Nanowires and commercial Ptlatinum/Carbon during Hydrogen Evolution Reaction process is evaluated by using the steady carbon fibre paper (CP) as a working electrode. Impressively, the chronoamperometric study indicates that, under the same conditions, the current density at as-synthesized Pt NWs/SLNi(OH)2 shows a considerably slower decay than that at Pt/C, pure Pt NWs and Pt NPs/SL-Ni(OH)2 both in 1 and 0.1 M POTASSIUM HYDROXIDE (Fig. 7c,d). Through analyzing data shown in Fig. 9c,d, several conclusions can be achieved about the stability performance of Pt NWs/SL-Ni(OH)2 catalysts. First of all, on the SL-Ni(OH)2 substrates, the ultrathin 1D Pt NWs have higher stability compared with Pt NPs. Pt NWs/SL-Ni(OH)2 preserves 95.7 and 98.3% of its initial activity in 1 M and 0.1 M POTASSIUM HYDROXIDE, respectively, after 4,000 s test, while Pt NPs/SL-Ni(OH)2 keeps 85.4 and 90.3% of the initial activity. The astonishing electrochemical stability of OneDimensional nanostructures have been demonstrated.

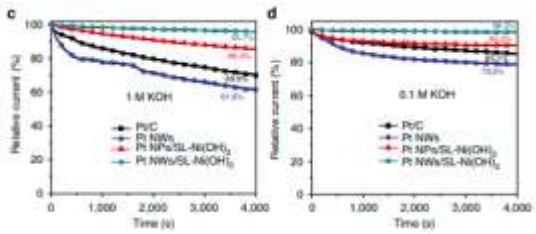


Figure 7 (c,d) - The current density is normalized by the electrochemical surface areas of Platinum (c,d) Normalized current-time (i–t) chronoamperometric responses for HER at Platinum NanoWires/SL-Ni(OH)2, Platinum NanoPores/SL-Ni(OH)2 Pt NWs and commercial Pt/C (20 wt.%) electrodes in 1 and 0.1 M POTASSIUM HYDROXIDE solution.

## III. MATHEMATICAL MODULATION AND SIMULATION OF HYDROGEN FUEL CELLS

### 3.1 Hydrogen Consumed and Current Produced

A hydrogen oxygen fuel cell with the reaction

$$H2 + O2 \rightarrow H2O$$

H2 here is treated as an ideal gas;
the molar flow rate is related to the volumetric flow rate via the ideal gas law:

$$\frac{dN}{dt} = \frac{P(dV/dt)}{RT}$$

The total amount of electricity produced is calculated by integrating the current load over the operation time

$$i = nF\frac{dN}{dt}$$

The total number of moles of H2 processed by the fuel cell is:

$$Q_{tot} = i_1 t_1$$

*International Journal of Engineering Applied Sciences and Technology, 2022*
**Vol. 7, Issue 4, ISSN No. 2455-2143, Pages 262-275**
Published Online August 2022 in IJEAST (http://www.ijeast.com)

$$N_{H2} = \frac{Q_{tot}}{nF}$$

If we take

R = 0.082 Ideal gas constant (L/atm/molK)
T = 333.15 Temperature
dV_dt = 0.005 Volumetric flow rate (L/min)
P = 3 atm
n = 2mol e- per mole fuel
F = 96487 Faraday's constant
T = 120 min

Then current ( I ) comes to be 1.77A
And moles of h2 used will be 3.95 moles

**3.2 The Activation Overpotential of PEM fuel cell**
The activation overpotential equation derived from the Butler-Volmer equation is:

$$\Delta V_{act} = \frac{RT}{\alpha F} \ln\left(\frac{i}{i_0}\right)$$

Using Butler-Volmer equation we can plot the variation between current density and temperature as a function of Activation loss.

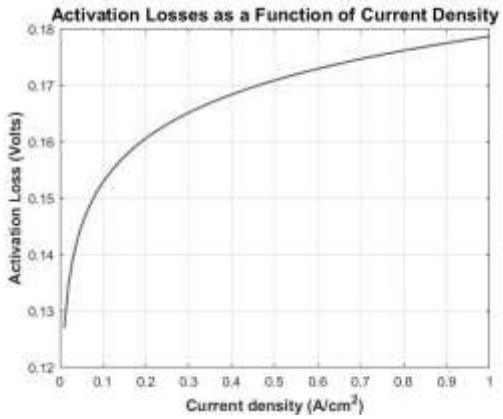


Figure 8 (a) – Plot showing Activation losses as a function of current desity VS current density

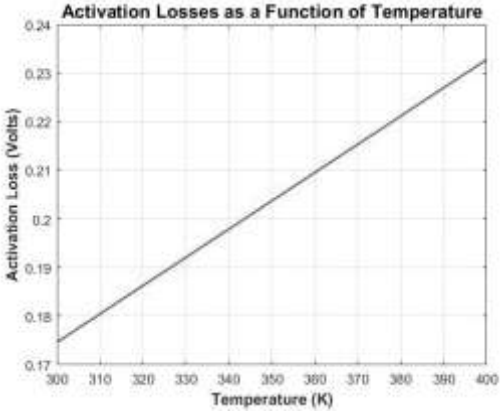


Fig 8 (b) – Plot showing Activation losses as a function of Temperature VS Temperature

**3.3 Ohmic Voltage Loss**
Calculating Rionic based upon electrolyte dimensions to calculate u ohmic.
The current of the fuel cell is:
I = iA

$$R = \frac{L}{\sigma A}$$

$$\upsilon_{ohmic} = I(R_{elec} + R_{ionic})$$

If this equation is calculated for thinner and thicker membranes, one will notice that the Ohmicloss is reduced with thinner membranes.
i = 0.7 Current density (A/cm^2)
A = 100 Area (cm^2)
L = 0.005 Electrolyte thickness (cm)
sigma = 0.1 Conductivity (ohms/cm)
R_elec = 0.00 Electrical resistance (ohms)

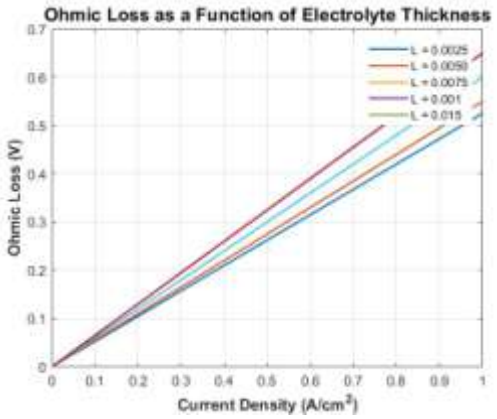


Figure 9 - Plot for showing variation in ohmic loss with increasing in membrane thickness.

*International Journal of Engineering Applied Sciences and Technology, 2022*
**Vol. 7, Issue 4, ISSN No. 2455-2143, Pages 262-275**
Published Online August 2022 in IJEAST (http://www.ijeast.com)

### 3.4 Ohmic loss due to Nafion membrane

The amount of water that the membrane can hold also depends upon the membrane pre-treatment. For example, at high temperatures, the water uptake by the Nafi on membrane is much lower due to changes in the polymer at high temperatures. The relationship between water activity on the faces of the membrane and water content can be described by:

$$\lambda = 0.043 + 17.18a_{water\_vap} - 39.85|a_{water\_vap}|^2 + 36|a_{water\_vap}|^3$$

Water uptake results in membrane swelling, which changes the membrane thickness along with its conductivity, the ionic conductivity (s) (in S/cm) to water content and the temp:

$$\sigma = (0.005139\lambda - 0.00326)\exp\left[1268\left(\frac{1}{303} - \frac{1}{T}\right)\right]$$

Since conductivity is proportional to resistance, the resistance of the membrane changes with water saturation and thickness. The total resistance of a membrane (Rm) is found by integrating the local resistance over the membrane thickness:

$$R_m = \int_0^{t_m} \frac{dz}{\sigma[\lambda(z)]}$$

The ohmic overvoltage due to the membrane resistance in this fuel cell is:

$$V_{ohm} = j \times R_m$$

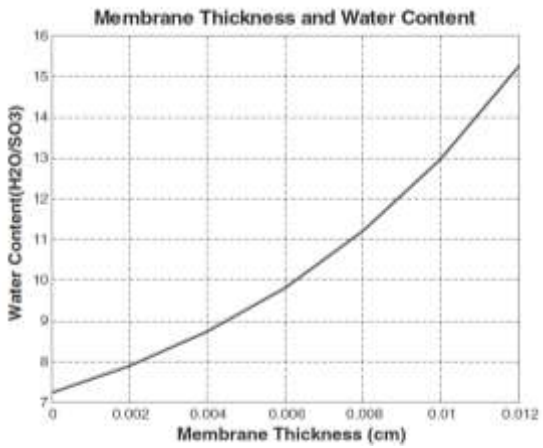


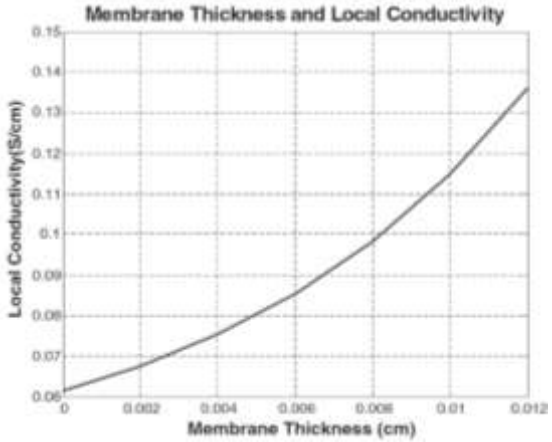


Figure 10 – Plot showing Membrane thickness and water content VS Membrane thickness (b) Plot showing Membrane thickness and Local Conductivity VS Membrane thickness

### 3.5 Water Injection Flow Rate

The water mass balance is

$$m_{H2O\_air\_in} + m_{H2O\_Inject} + m_{H2O\_gen} = m_{H2O\_in\_air\_out}$$

In order to calculate the amount of water in air, the saturation pressure needs to be calculated. To calculate the saturation pressure (in Pa) for any temperature between 0 °C and 100 °C:

$$p_{vs} = e^{aT^{-1}+b+cT+dT^2+eT^3+f\ln(T)}$$

where a, b, c, d, e, and f are the coefficients.

$a = -5800.2206$, $b = 1.3914993$, $c = -0.048640239$, $d = 0.41764768 \times 10^{-4}$, $e = -0.14452093 \times 10^{-7}$, and $f = 6.5459673$

The amount of water in air can be calculated:

$$m_{H2O,ainin} = \frac{S_{O2}}{x_{O2}} \frac{M_{H2O}}{nF} \frac{\phi_{ca} P_{vs(T_{ca,in})}}{P_{ca} - \phi_{ca} P_{vs(T_{ca,in})}} I \cdot n_{cell}$$

Water generated is:

$$m_{H2O,gen} = \frac{I}{nF} M_{H2O}$$

*International Journal of Engineering Applied Sciences and Technology, 2022*
**Vol. 7, Issue 4, ISSN No. 2455-2143, Pages 262-275**
Published Online August 2022 in IJEAST (http://www.ijeast.com)

Water vapor in air out is:

$$m_{H2O,Air,out,V} = \left[\left(\frac{S_{O2} - r_{O2,in}}{r_{O2,in}}\right)\frac{M_{H2O}}{4F}\frac{P_{vs}T_{air,out}}{P_{ca} - \Delta P_{ca} - P_{vs}T_{air,out}} I \cdot n_{cell}\right]$$

By putting
T_H2_in = 293.15 Hydrogen inlet temperature
T_air_out = 353.15 Air inlet temperature
phi = 0.5 Relative humidity
P = 120 Pressure (kPa)
n_cell = 1 No. of cells
Power = 500Power (watts)
V = 0.7 Voltage (V)
M_H2O = 18.015 Molecular weight of water
F = 96,485 Faraday's law
S_O2 = 2 Oxygen stoichiometric ratio
r_O2 = 0.2095 Mole fraction of oxygen in air

we get the out flow as 0.22317 g/s

**3.6 Coolant Mass Flow Rate**
The solid surface temperature at the cooling channel exit is:

$$Q = L_{plate} P_{cs} k_{solid} \frac{(T_{edge} - T_{surface})}{t_{bc}}$$

The hydraulic diameter is given by:

$$D_h = \frac{4A_{cross\text{-}section}}{P_{channel}} = \frac{4dw}{2(d+w)}$$

The heat transfer coefficient is then calculated:

$$h = 8.23\frac{k_{gas}}{D_h}$$

The heat transfer coefficient is used to determine the gas exit temperature:

$$T_{gas} = T_{surface} - \frac{Q_{cell}}{hLP_{channel}}$$

The air mass flow rate can be determined by setting Tcoolant,out = Tgas.

$$\dot{m}_{coolant} = \frac{Q_{cell}}{C_p T_{coolant,out} - T_{coolant,in}}$$

w_chan = 0.001 Channel width (m)
t_chan = 0.10 Channel thickness (m)
L_bpp = 0.10 Bipolar plate length (m)
t_bpp_cell = 0.004 Bipolar plate and cell thickness (m)
T_max = 353.15 Maximum operating temperature (K)
T_cool = 295.15 Cooling temperature (K)
Q_cell = 2 Heat generated per cell (W)
cp = 1.0 Specific heat (J/gK)
k_gas = 0.026 Thermal Conductivity of gas (W/mK)
k_solid = 20 Thermal Conductivity of solid (W/mK)

by putting the above values, we get a mass flow rate of the coolant to about 0.035 g/s.

**3.7 Energy Balances**
Formula of energy balance is:

$$H_{H2,in} + H_{Air,in} + H_{H2O\_Air,in} = H_{Air,out} + H_{H2O\_Air,out} + W_{el}$$

The energy flows are:

Hydrogen in:

$$H_{H2,in} = m_{H2,in}\left(c_{p,H2}T_{in} + h^0_{HHV}\right)$$

Air in:

$$H_{Air,in} = m_{Air,in}c_{p,Air}T_{in}$$

The amount of water produced

I = P/V

$$m_{H2O,gen} = \frac{I}{2F}M_{H2O}$$

The water balance is:

$$m_{H2O\_Air,in} + m_{H2O,gen} = m_{H2O\_Air,out}$$

Water vapor in air out:

$$H_{H2O\_Air,out} = m_{H2O\_Air,out} \times \left(c_{p,H2O}T_{out} + h^0_{fg}\right)$$

Final Energy balance:

*International Journal of Engineering Applied Sciences and Technology, 2022*
**Vol. 7, Issue 4, ISSN No. 2455-2143, Pages 262-275**
Published Online August 2022 in IJEAST (http://www.ijeast.com)

$$H_{H2,in} + H_{Air,in} + H_{H2O\_Air,in} = H_{Air,out} + H_{H2O\_Air,out} + W_{el}$$

So with this we can find enthalpy of air in the system.

### 3.8 Transient Conduction through Plate

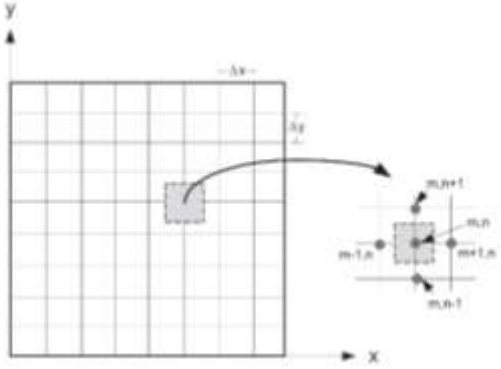


Figure 11 (a) pictorial representation of nodes

For the uniform distribution of nodes. The location of each node (xi) is:

$$x_i = \frac{(i-1)}{(N-1)} L$$

Where N is the number of nodes used for the simulation. The distance between adjacent nodes (Δx) is:

$$\Delta x = \frac{L}{N-1}$$

Energy balances have been defined around each node (control volume).
The control volume for the first, last, and an arbitrary, internal node is shown in Figure 11(a). Each control volume has conductive heat transfer with
each adjacent node in addition to energy storage:

$$\dot{q}_{LHS} + \dot{q}_{RHS} = \frac{dU}{dt}$$

And the value of $q_{LHS}$ and $q_{RHS}$is:

$$\dot{q}_{LHS} = \frac{kA(T_{i-1} - T_i)}{\Delta x}$$

$$\dot{q}_{RHS} = \frac{kA(T_{i+1} - T_i)}{\Delta x}$$

Here A is the area of the plate. The rate of energy storage is the product of the time rate of change of the nodal temperature and the thermal mass of the control volume:

$$\frac{dU}{dt} = A\Delta x\rho c \frac{dT_i}{dt}$$

Therefore :

$$A\Delta x\rho c \frac{dT_i}{dt} = \frac{kA(T_{i-1} - T_i)}{\Delta x} + \frac{kA(T_{i-1} - T_i)}{\Delta x}$$

Solving for the time rate of the temperature change:

$$\frac{dT_i}{dt} = \frac{k}{\Delta x^2 \rho c}(T_{i-1} + T_{i+1} - 2T_i) \quad \text{for} \quad i = 2 \ldots (N-1)$$

$$\frac{dT_N}{dt} = \frac{2k}{\rho c \Delta x^2}(T_{N-1} - T_N) + \frac{2h}{\Delta x \rho c}(T_i - T_N)$$

It should be noted that the equations provide the time rate of change for the temperature of every node given the temperatures of the nodes. The energy balance for each control volume provides an equation for the time rate of change of the temperature in terms of the temperature. Therefore, the energy balance written for each control volume has a set of equations for the time rate of change.

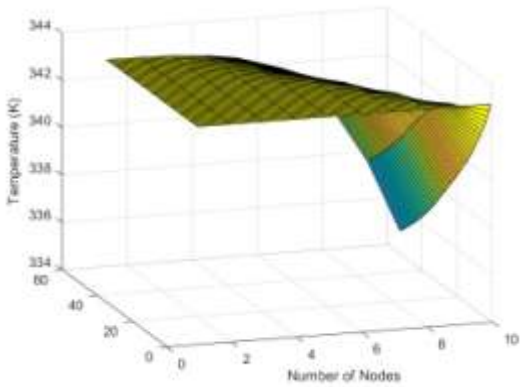


Fig 11 (b) - Temperature VS number nodes for a polymer layer

The simulation model of the power supply based PEMFC is developed. During the modeling in MATLAB /Simulink environment the influence of the following fuel cell input parameters such as fuel flow rate, air flow rate and operating

*International Journal of Engineering Applied Sciences and Technology, 2022*
**Vol. 7, Issue 4, ISSN No. 2455-2143, Pages 262-275**
Published Online August 2022 in IJEAST (http://www.ijeast.com)

temperature changing on voltage and current of the PEMFC itself and of the load is defined. Power supply is considered apart from the chemical reactions is considered. The model is prepared in MATLAB/Simulink 2020a version using the fuel cell stack present in Sims cape library electrical section.

**3.9 Model Description**

The model represents a proton exchange fuel cell when the parameters such as pressures, temperature, compositions and flow rates of fuel and air vary. These variations affect the open circuit voltage (Eoc), the exchange current (i0), and the Tafel slope (A). Eoc, i0 and A are modified as follows:

$$E_{oc} = K_c E_n$$

$$i_0 = \frac{zFk\left(P_{H_2} + P_{O_2}\right)\Delta v}{Rh} e^{\frac{-\Delta G}{RT}}$$

$$A = \frac{RT}{z\alpha F},$$

Where:
R = 8.3145 J/(mol K)
F = 96485 A s/mol
z = Number of moving electrons
En = Nernst voltage, which is the thermodynamics voltage of the cells and depends on the temperatures and partial pressures of reactants and products inside the stack (V)
α = Charge transfer coefficient, which depends on the type of electrodes and catalysts used
PH2 = Partial pressure of hydrogen inside the stack (Pa)
PO2 = Partial pressure of oxygen inside the stack (Pa)
k = Boltzmann's constant = 1.38 × 10–23 J/K
h = Planck's constant = 6.626 × 10–34 J s
Δv = Activation barrier volume factor (m3). The size of activation barrier (ΔG) is computed assuming Δv = 1 m3.
ΔG = Size of the activation barrier which depends on the type of electrode and catalyst used (J/mol)
T = Temperature of operation (K)
Kc = Voltage constant at nominal condition of operation

The equivalent circuit is the same as for the simplified model, except that the parameters:

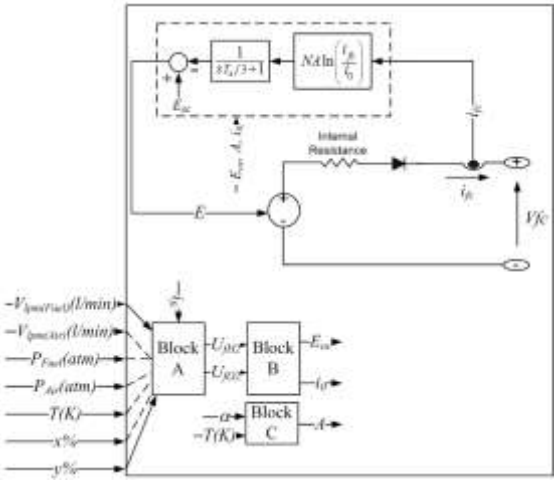

Fig 12: Equivalent circuit of a fuel cell stack

The rates of conversion (utilizations) of hydrogen (UfH2) and oxygen (UfO2) are determined in Block A as follows:

$$U_{fH_2} = \frac{n^r_{H_2}}{n^{in}_{H_2}} = \frac{60000RTNi_{fc}}{zFP_{\text{fuel}}V_{lpm(\text{fuel})}x\%}$$

$$U_{fO_2} = \frac{n^r_{O_2}}{n^{in}_{O_2}} = \frac{60000RTNi_{fc}}{2zFP_{\text{air}}V_{lpm(\text{air})}y\%}$$

Where:

Pfuel = Absolute supply pressure of fuel (atm)
Pair = Absolute supply pressure of air (atm)
Vlpm(fuel) = Fuel flow rate (l/min)
Vlpm(air) = Air flow rate (l/min)
x = Percentage of hydrogen in the fuel (%)
y = Percentage of oxygen in the oxidant (%)
N = Number of cells
The 60000 constant comes from the conversion from the liter/min flow rate used in the model to m3/s (1 liter/min = 1/60000 m3/s).

The partial pressures and the Nernst voltage are determined in Block B as follows:

$$P_{H_2} = \left(1 - U_{f_{H_2}}\right)x\%P_{\text{fuel}}$$

$$P_{H_2O} = \left(w + 2y\%U_{f_{O_2}}\right)P_{\text{air}}$$

$$P_{O_2} = \left(1 - U_{f_{O_2}}\right)y\%P_{\text{air}}$$

And

*International Journal of Engineering Applied Sciences and Technology, 2022*
**Vol. 7, Issue 4, ISSN No. 2455-2143, Pages 262-275**
Published Online August 2022 in IJEAST (http://www.ijeast.com)

$$E_{oc} = \begin{cases} 1.229 + (T - 298)\frac{-44.43}{2F} + \frac{RT}{2F}\ln\left(P_{H_2}P_{O_2}^{1/2}\right) & \text{when } T \le 100°C \\ 1.229 + (T - 298)\frac{-44.43}{2F} + \frac{RT}{2F}\ln\left(\frac{P_{H_2}P_{O_2}^{1/2}}{P_{H_2O}}\right) & \text{when } T > 100°C \end{cases}$$

Where:

PH2O = Partial pressure of water vapor inside the stack (atm)
w = Percentage of water vapor in the oxidant (%)
From the partial pressures of gases and the Nernst voltage, the new values of the open circuit voltage (Eoc) and the exchange current (i0) can be calculated.

In the PEMFC, there are different kinds of voltage losses, each affecting a certain area of the current-voltage characteristics. The current-voltage characteristics of the fuel cell stack are shown in Figure 16.

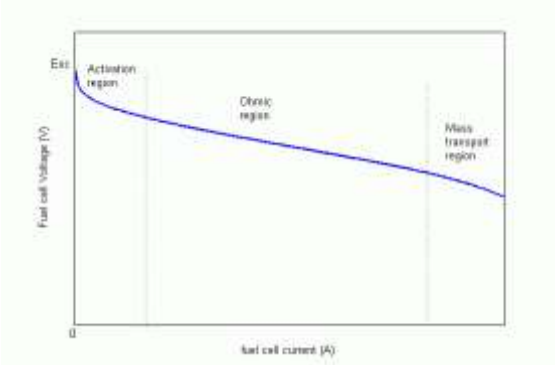

Fig 13: I-V characteristics of PEMFC

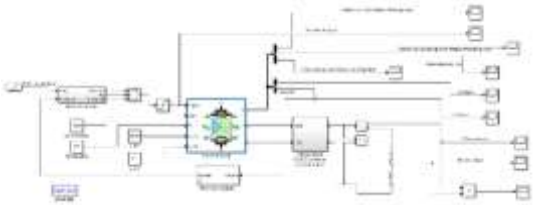
Fig 14: Model made in MATLAB 2020a

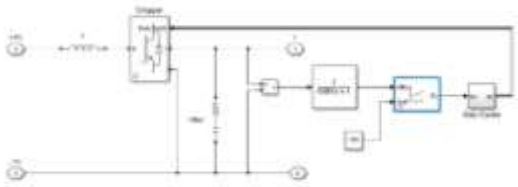
Fig 15: 100Vsc Boost DC/DC convertor

**3.10 Working Of Fuel Cell Stack:**
To conduct and collect information/data on PEMFC we have simulated it in MATLAB/Simulink 2020a environment. Modelling in this environment will provide obtaining the data on the basis of which a conclusion concerning the degree of the change influence of every input parameter on the output characteristics of the fuel with a cell proton exchange membrane can be made.
Simulation Model PEMFC station is shown in Fig. 15.
A DC-to-DC converter is an electronic circuit which converts a source of Direct Current (DC) from one voltage level to another. It is a type of electric power
converter. Power levels range from very low (small batteries) to very high (high-voltage power transmission). The DC-to-DC converter that used is shown in Fig. 16.
This DC-to-DC convertor will pull up the current to about 100Vdc and try to stabilize it at that point.
We have used a fuel cell stack with 65 stacks of proton exchange fuel cell and its stack voltage-current characteristics and power-current characteristics is show in fig 16.
The stack voltage vs current is shown in Fig. 16. As shown in this figure, this curve represents the value of voltage vs current. This simulation is inside the stack. For every current from 0A to 250A, the voltage is shown as below.

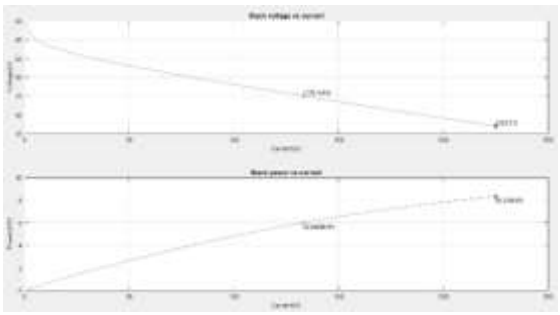
Fig 16: voltage-current and power-current characteristics of PEMFC

Fig. 17 shows the stack power vs current. As seen in this figure the current start at 0A and increases 250A. The maximum power is 8.325KW.
The changing rate of fluid flow is done with the help of a feedback. The fuel flow control (Flow rate regulator) is used to provide the fuel consumption at a constant level until it is off, then there is an increase in the fuel flow rate to a maximum value of 85l/min.

**3.11 Simulation Result:**

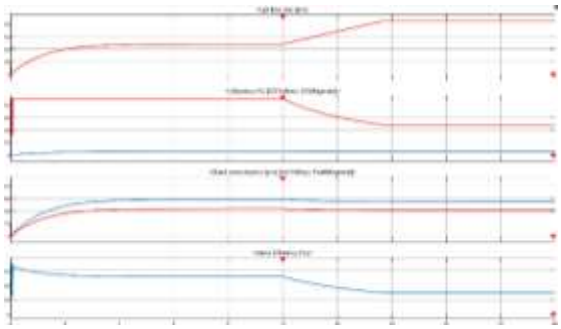
Fig 17: Fuel flow rate, utilization, stack consumption, stack efficiency

*International Journal of Engineering Applied Sciences and Technology, 2022*
**Vol. 7, Issue 4, ISSN No. 2455-2143, Pages 262-275**
Published Online August 2022 in IJEAST (http://www.ijeast.com)

After simulation the results are shown in fig. 17, 18, 19. In the figure 18 x axis is time in seconds and the y axis is flow rate of the fuel(Hydrogen), completely utilization% of air and H2, Stack consumption of air and H2, and the stack efficiency.

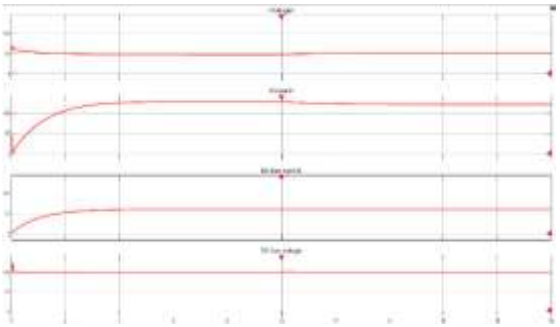

Fig 18: voltage, current, DC bus current, DC bus voltage

The output of the stack is shown in Fig. 18. In this figure, the voltage, current, DC bus voltage and DC bus current is shown.

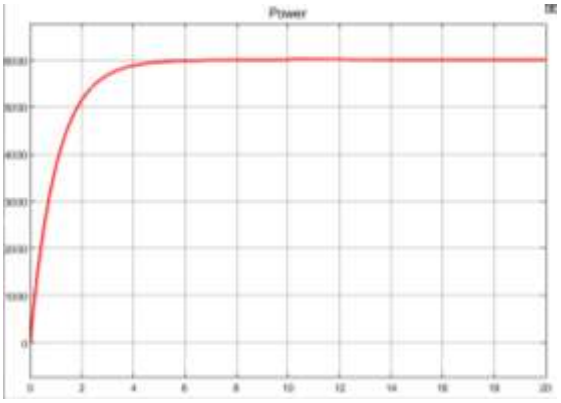


Fig 19: Time-Power Characteristics of PEMFC

As shown in Fig. 19, after 6 seconds, the output is obtained. In this figure, the X-coordinate is Time (s) and Y-coordinate is power (W).

## IV. RESULTS AND CONCLUSION

This paper presented the different research domains for improving the catalyst's performance. It is found that the performance of the catalyst is mainly dependent on two factors:
① in a given area the number of active sites
② the geometrical structure and intrinsic activity of the active sites.

A possible way to enhance the performance of the catalysts is by introducing Platinum Nanowires which increases the HER activity.
The mathematical and modulation of the Hydrogen Fuel Cells have shown the relationship between different parameters of the fuel cells. Each of these parameters plays an vital role for determining the efficiency of the hydrogen fuel cell.
We believe that this paper will help researchers to implement the technologies mentioned and will help them to increase the efficiency of Hydrogen Fuel Cells.

**Acknowledgment**
This work was supported by Department of Chemical Engineering,Vishwakarma Institute of Technology, Pune. The authors thanks to Mr. Shrikaant Kulkarni for sponsoring the project and guiding throughout.

## V. REFERENCES

[1] Zhang Zu, Wang, (2013), , X. Formamide: an efficient solvent to synthesize water-soluble and sub-ten-nanometer nanocrystals. Nanoscale 5, 4495–4505.
[2] Wu, J., Gross, A. & Yang, (2011) H. Shape and composition-controlled platinum alloy nanocrystals using carbon monoxide as reducing agent. Nano Lett. 11, 798–802.
[3] Mclntyre, N. S. & Cook, M. G.(1975) X-ray photoelectron studies on some oxides and hydroxides of cobalt, nickel, and copper. Anal. Chem. 47, 2208–2213.
[4] Choi, (2013)S.-I. et al. Synthesis and characterization of 9 nm Pt-Ni octahedral with a record high activity of 3.3A/mgPt for the oxygen reduction reaction. Nano Lett. 13, 3420–3425.
[5] Park, K.-W.(2002) et al. Chemical and electronic effects of Ni in Pt/Ni and Pt/Ru/Ni alloy nanoparticles in methanol electrooxidation. J. Phys. Chem. B 106, 1869–1877.
[6] Wagner, C. D., Riggs, W. M., Davis, L. E. & Moulder, J. F. (1979)Handbook of X-ray Photoelectron Spectroscopy 40–41 (Perkin-Elmer Corporation, MN, USA)
[7] Huang, X. et al. (2013) Solution-phase epitaxial growth of noble metal nanostructures on dispersible single-layer molybdenum disulfide nanosheets. Nat. Commun. 4, 1444.
[8] Chen, Z., Waje, M., Li, W. & Yan, Y. (2014) Supportless Pt and PtPd nanotubes as electrocatalysts for oxygen-reduction reactions. Angew. Chem. Int. Ed. 46, 4050–4063 (2007). 53. Chen, G. et al. Interfacial effects in iron-nickel hydroxide-platinum nanoparticles enhance catalytic oxidation. Science 344, 495–499.
[9] Huang, X., Qi, X., Boey, F. & Zhang, H. (2012) Graphene-based composites. Chem. Soc. Rev. 41, 666–686.
[10] Huang, X. (2011) Synthesis of hexagonal close-packed gold nanostructures. Nat. Commun. 2, 292.
[11] Koenigsmann, C. & Wong, S. S. (2011), One-dimensional noble metal electrocatalysts: a promising structural paradigm for direct methanol fuel cells. Energy Environ. Sci. 4, 1161–1176.

[12] Hu, S. & Wang, X. (2013) Ultrathin nanostructures: smaller size with new phenomena. Chem. Soc. Rev. 42, 5577–5594.

[13] Teng, X., Han, W.-Q., Ku, W. &Hu¨cker, M. (2008) Synthesis of ultrathin palladium and platinum nanowires and a study of their magnetic properties. Angew. Chem. 120, 2085–2088.

[14] Koenigsmann, C., Zhou, W., Adzic, R. R., Sutter, E. & Wong, S. S. (2010) Sizedependent enhancement of electrocatalytic performance in relatively defectfree, processed ultrathin platinum nanowires. Nano Lett. 10, 2806–2811.

[15] Song, Y. (2007), Synthesis of platinum nanowire networks using a soft template. Nano Lett. 7, 3650–3655.

[16] Ru, L. (2013) Biomimetic synthesis of an ultrathin platinum nanowire network with a high twin density for enhanced electrocatalytic activity and durability. Angew. Chem. Int. Ed. 52, 12577–12581.

[17] Sun, S., Jaouen, F. &Dodelet, J.-P. (2008) Controlled growth of Pt nanowires on carbon nanospheres and their enhanced performance as electrocatalysts in PEM fuel cells. Adv. Mater. 20, 3900–3904.

[18] Zhang, L., Li, N., Gao, F., Hou, L. & Xu, Z (2012). Insulin amyloid fibrils: an excellent platform for controlled synthesis of ultrathin superlong platinum nanowires with high electrocatalytic activity. J. Am. Chem. Soc. 134, 11326–11329.

[19] Xiao, Q., Cai, M., Balogh, M. P., Tessema, M. M. & Lu, Y. (2012) Symmetric growth of Pt ultrathin nanowires from dumbbell nuclei for use as oxygen reduction catalysts. Nano Res. 5, 145–151.

[20] Xia, B. Y., Wu, H. B., Yan, Y., Lou, X. W. & Wang, X. (2013) Ultrathin and ultralong single-crystal platinum nanowire assemblies with highly stable electrocatalytic activity. J. Am. Chem. Soc. 135, 9480–9485.

[21] K. Belmokhtar. (2013), "Modeling and fuel flow dynamic control of proton exchange membrane fuel cell," Power Engineering, Energy and Electrical Drives (POWERENG), 2013. Fourth International Conference on, IEEE.

[22] M. Ehsani, Y. Gao, and A. Emadi. (2010), 'Modern Electric, Hybrid Electric and Fuel Cell Vehicles, Fundamentals, Theory and Design', CRC Press.

[23] G. Bhansali, Kumar R. (2014) "Design analysis and dynamic control of PEM fuel cell for standalone applications," Electrical, Electronics and Computer Science (SCEECS), 2014 IEEE Students' Conference on. – IEEE.

[24] Ceraolo M., Miulli C., Pozio A., (2003), "Modelling static and dynamic behaviour of proton exchange membrane fuel cells on the basis of electro-chemical description," J. Power Sources, vol. 113, no. 1, pp. 131-144.

[25] Sorenson Bent (2016), 'Comparison between hydrogen fuel cell vehicles and bio-diesel vehicles', Roskilde University, Institute of Mathematics and Physics, Energy & Environment Group Universities.

[26] Thanapalan Kary, Williams Jonathan, Premier Giuliano, Guwy Alan (2015), 'Design and Implementation of Renewable hydrogen fuel cell vehicles', Sustainable Environment Research Centre (SERC), Renewable Hydrogen Research & Demonstration Centre, University of Glamorgan, Baglan Energy Park, Baglan, Port Talbot, UK. Implementation of Renewable hydrogen fuel cell vehicles', Sustainable Environment Research Centre (SERC), Renewable Hydrogen Research & Demonstration Centre, University of Glamorgan, Baglan Energy Park, Baglan, Port Talbot, UK

[27] Pollet B.G., Kendall K., Dhir A., Stafell I., Bujalski W., (2010) 'Hydrogen Fuel Cell Battery Electric Vehicles (HFCBEV) vs. Battery Electric Vehicles (BEV) - A Birmingham Experience'18th World Hydrogen Energy Conference

[28] Francesch Judit Anton. (2014), Bachelor thesis Hydrogen Fuel Cell Vehicles' Vienna University of technology.

[29] Garland Nancy, Papageorgopoulos Dimitrios, Stanford Joseph, (2012), 'Hydrogen and fuel cell technology: Progress, challenges, and future directions' Fuel Cells Science &Technology, US Department of Energy, Washington, DC 20585-0121, USA .

[30] Jakupca Ian, (2019), 'NASA Fuel Cell and Hydrogen Activities', Department of Energy Annual Merit Review.

[31] Jordan Ing. 'Overview of hydrogen and fuel cell technologies', Institut für Kern- und Energietechnik, Forschungszentrum Karlsruhe GmbH.

[32] Potera Carol, (2007), 'Beyond Batteries' Environmental Health Perspectives, Volume115 | Number 1.

[33] TayyarDzhafarov and Sureyya Aydin Yuksel, 'Nano-Porous Silicon-Based Mini Hydrogen Fuel Cells', Institute of Physics, Azerbaijan National Academy of Sciences, Baku Department of Physics, Yildiz Technical University, 34210 Istanbul, Azerbaijan, Turkey.

[34] Arat HüseyinTuran, Bahattin Tanc, Özaslan Nevzat, (2020), 'Sustainability Analyses for Hydrogen Fuel Cell Electric Vehicles' , IntechOpen 2020.

[35] Peng Lishan, Wei Zidong. (2019), 'Catalyst Engineering for Electrochemical Energy Conversion from Water to Water: Water Electrolysis and the Hydrogen Fuel Cell', Chongqing Key Laboratory of Chemical Process for Clean Energy and Resource Utilization, School of Chemistry and Chemical Engineering, Chongqing University, Chongqing 400044, China.

[36] Jervis Rhodri. (2015), 'Development of Novel Alloy Electrocatalysts for the Hydrogen Oxidation Reaction in Alkaline Media and their Application to Low Temperature Fuel Cells', A thesis submitted for the partial fulfilment of the requirements for the degree of Doctor of Philosophy at University College London, Department of Chemical Engineering, London.

[37] Yin Huajie, Zhao Shenlong, Zhao Kun, Muqsit Abdul, Tang Hongjie, Chang Lin, Zhao Huijun, Gao Yan, Zhiyong Tang. (2014), 'Ultrathin platinum nanowires grown on single-layered nickel hydroxide with high hydrogen evolution activity', Laboratory for Nanosystem and Hierarchy Fabrication, National Center for Nanoscience and Technology, Beijing.

[38] P´erezMaronda. (2018), 'Impact of Pt Loading on Proton Exchange Membrane Hydrogen Fuel Cells Performance', A thesis submitted in partial fulfillment of the requirements for the degree of Renewable Energy Master degree, Department of Mechanical Engineering University of Alberta, Xavier.

[39] Jack Zhang,(2011), 'Effects on Hydrogen Adsorption and Activation on Platinum in a Fuel Cell Catalyst', Clemson University TigerPrints.

[40] Friedla Jochen, Stimming Ulrich. (2013), Model Catalyst Studies on Hydrogen and Ethanol Oxidation for Fuel Cells', Newcastle University, Electrochimica Acta.

[41] Singh Ramesh, Davydova Elena, Doughlin John, Godoy Andreas, Haiyan Tan, Bellini Marco, Allen Bryan, Miller Hamish, Dekel Dario. (2020) 'Synthesis of CeOx-Decorated Pd/C Catalysts by Controlled Surface Reactions for Hydrogen Oxidation in Anion Exchange Membrane Fuel Cells', Published by WILEY-VCH Verlag GmbH & Co. KGaA, Weinheim.

[42] SivaprakashSengodana, Lana Rong, DongweiDua, Humphreysa John, Xua Wei, Wang Huanting. (2018) ShanwenTaoa, 'Advances in reforming and partial oxidation of hydrocarbons for hydrogen production and fuel cell applications', Renewable and Sustainable Energy Reviews, b Department of Chemical Engineering, Monash University, Clayton, Victoria 3800, Australia.

[43] Brandon Negel, Thompsett Dave. (2005), 'Fuel Cells Compendium', Elsevier.

[44] Palo Daniel, Dagel Robert and Holland Jamie. (2007), 'Methanol Steam Reforming for Hydrogen Production', Pacific Northwest National Laboratory, , Richland, Washington 99354.

[45] Chen Ping, Zhu Min. (2008), 'Recent progress in hydrogen storage', Materialstoday, Volume 11.

[46] Dicks Andrew and Larminie James. (2003), 'Fuel cells explained', Second Edition, John Wiley & Sons Ltd, The Atrium, Southern Gate, Chichester, West Sussex PO19 8SQ, England.

[47] Choudhary T.V., Sivadinarayana C. and Goodman D.W. (2001), 'Catalytic ammonia decomposition: COx-free hydrogen production for fuel cell applications', Catalysis Letters Vol. 72, No. 3-4, Chemistry Department, Texas A&M University, PO Box 30012, College Station, TX 77842-3012, USA.

[48] Brown Lee (2001), 'A comparative study of fuels for on-board hydrogen production for fuel-cell-powered automobiles', International Journal of Hydrogen Energy 26, Engineering Sciences and Applications Division, Los Alamos National Laboratory, USA.

[49] Zuttel Andreas. (2004), 'Hydrogen storage methods', Naturwissenschaften, Physics Department, University of Fribourg, Prolles, 1700 Fribourg, Switzerland.

[50] Züttel Andreas. (2003), 'Materials for hydrogen storage', Materialstoday, Physics Department, University of Fribourg, Pérolles CH-1700 Fribourg Switzerland.

[51] Volodymyr A. Yartys and Mykhaylo V Lototskyy. (2003) 'An overview of hydrogen storage methods', Hydrogen Materials Science and Chemistry of Carbon Nanomaterials, NATO Advanced Research Workshop on Hydrogen Materials Science and Chemistry of Carbon Nanomaterials Sudak, Crimea, Ukraine 14-20.

[52] https://www.energy.gov/eere/office-energy-efficiency-renewable-energy, Fuel Cell technologies program, Energy Efficiency and Renewable Energy, US Department of Energy January 2011.